Front. Energy
https://doi.org/10.1007/s11708-019-0608-0

RESEARCH ARTICLE

Zhaorui ZHAO, Bao YANG, Ziwen XING

Modeling analysis on solar steam generator employed in multi-effect distillation (MED) system

Abstract Recently the porous bilayer wood solar collectors have drawn increasing attention because of their potential application in solar desalination. In this paper, a thermodynamic model has been developed to analyze the performance of the wood solar collector. A modeling analysis has also been conducted to assess the performance and operating conditions of the multiple effect desalination (MED) system integrated with the porous wood solar collector. Specifically, the effects of operating parameters, such as the motive steam temperature, seawater flow rate, input solar energy and number of effects on the energy consumption for each ton of distilled water produced have been investigated in the MED desalination system combined with the bilayer wood solar steam generator. It is found that, under a given operating condition, there exists an optimum steam generation temperature of around 145°C in the wood solar collector, so that the specific power consumption in the MED system reaches a minimum value of 24.88 kWh/t. The average temperature difference is significantly affected by the solar heating capacity. With the solar capacity increasing from 50 kW to 230 kW, the average temperature difference increases from 1.88°C to 6.27°C. This parametric simulation study will help the design of efficient bilayer wood solar steam generator as well as the MED desalination system.

Received Jul. 18, 2018; accepted Sept. 27, 2018; online Jan. 18, 2019

Zhaorui ZHAO (✉)
Department of Energy and Power Engineering, Xi'an Jiaotong University, Xi'an 710049, China; Center for Environmental Energy Engineering (CEEE), Department of Mechanical Engineering, University of Maryland, College Park, MD 20742, USA
E-mail: smile90613@163.com

Ziwen XING
Department of Energy and Power Engineering, Xi'an Jiaotong University, Xi'an 710049, China

Bao YANG
Center for Environmental Energy Engineering (CEEE), Department of Mechanical Engineering, University of Maryland, College Park, MD 20742, USA

Keywords solar energy, steam generating, multi-effect desalination

1 Introduction

Water scarcity has become a serious issue, especially for the inland countries, the Northern Africa, and the Western Asia [1,2]. Desalination is a process where the salt is removed from seawater to produce fresh water. The desalination process consumes energy, such as electrical, thermal, mechanical, or chemical energy [3]. Thermal desalination is more suitable in areas where electricity is insufficient or uneconomical but thermal energy, for example, solar energy, geothermal energy, or bio-thermal energy, is accessible [4–8]. Considerate work has been performed to develop and analyze thermal desalination systems. Darwish et al. have analyzed a number of feed water arrangements in multiple effect desalination (MED) systems including the forward, backward, parallel, and mixed feed cycles [9]. Zhang et al. have reviewed the application of solar energy in water treatment processes, where the cycle configuration and component development in thermal desalination systems are discussed [10,11]. Simulations have also been conducted on the characteristics, performance, and operation strategy of parabolic trough DSG loop in recirculation mode and solar power plant [12,13]. Bataineh have investigated the annual performance of multi-effect desalination plant employing a solar steam generation one [14]. Sharaf et al. have performed a case study on multi effect distillation-vapor compression desalination system which has a capacity of distillate products of 4545 m^3 per day [15]. Additionally, the MED-TVC is proved to be of a high performance ratio and a low maintenance cost, which is promising in utilization in low compression ratio MED systems and could reduce the amount of high pressure steam requirement at the same amount of distilling fresh water [16–18]. The combination of the MED cycle and the solar collector is a mainstream for economic desalination systems.

Traditional solar steam generators work for dilute salt water where the salt concentration is often less than 5%. However, the water produced from oil and gas wells has a much higher salinity (> 10%). Recently, porous bilayer wood solar collectors which have natural micro-channels for capillary water transport have drawn increasing attention because of their potential application in solar desalination of water with a high salinity [19]. Experimental results have shown that bilayer solar collectors exhibit distinct properties such as a rapid water transport and evaporation, a high light absorption (≈ 99%), a low thermal conductivity to avoid thermal loss, and a long-term stability in seawater without salt accumulation [20–22]. Simulation and experimental researches have also been conducted on solar collectors employed in desalination systems [23,24]. In this paper, a thermodynamic model is developed to analyze the performance of the bilayer wood solar collector. Besides, a modeling analysis is conducted to assess the performance and operating conditions of the MED system integrated with the porous wood solar collector.

2 Bilayer wood solar collector

2.1 Configuration of the bilayer wood solar collector

Figure 1 shows the schematic of the bilayer wood solar collector for steam generation. The bilayer wood has interconnected channels (fiber tracheids and lumina with diameters in the tens of micrometers) within the top "light-absorbing" layer as well as the bottom "water pumping" layer. There is a perfect microstructural match at the interface between the carbonized wood for light absorption and natural wood section. As the sun heats up the black top-layer of the wood, water is drawn up through the natural channels of the wood and turns into vapor.

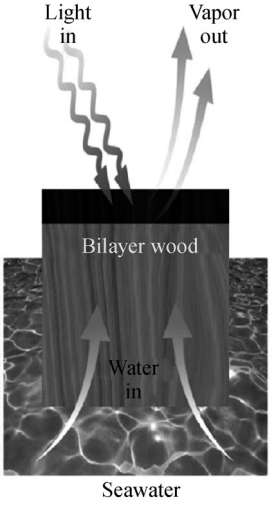

Fig. 1 Schematic of the bilayer wood solar collector for steam generation

Figure 2 illustrates the configuration of the solar steam generator. This steam generator is composed of a seawater chamber and a steam chamber. Thermal isolation layers are required between the generator and the ambient, and between the seawater chamber and steam chamber. The porous bilayer wood solar collector is inserted between the two chambers. An optic concentration device such as lens is employed to focus solar light on the top layer of the bilayer wood evaporator. Seawater flows in through the inlet of the seawater chamber, whose pressure and temperature depends on the requirement of the steam produced. The steam can be produced through the bilayer evaporator under solar irradiation

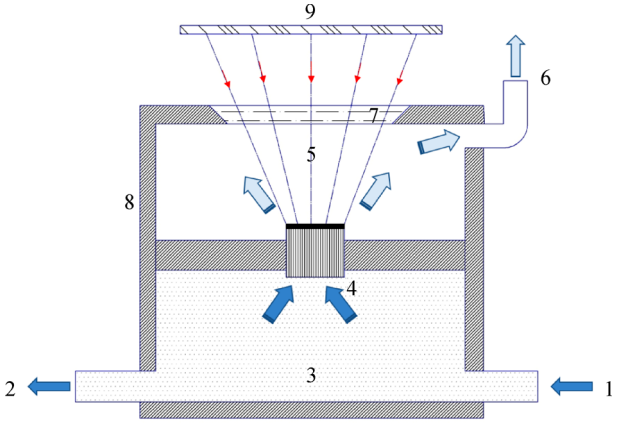

1—seawater inlet, 2—brine outlet, 3—seawater chamber, 4—bilayer wood evaporator, 5—steam chamber, 6—high pressure steam outlet, 7—glass window, 8—thermal isolation layer, 9—optic concentration device

Fig. 2 Schematic of a solar steam generator with the bilayer wood collector under direct solar heating

2.2 Modeling of bilayer wood solar steam generation

As shown in Fig. 3, the steam generation process in the bilayer wood can be divided into three closely connected thermodynamic processes. At first, seawater flows in the microchannel between wood fibers, whose temperature increases gradually to the saturation temperature at the top of the solar absorption layer. In the first process, the seawater, which is at a relatively low temperature determined by the inlet temperature after the preheating, may absorb heat to increase in temperature until reaching the saturation point. Meanwhile, it flows along the fiber tubes of the wood material to reach the top of the wood layer. Then, in the second process, the seawater evaporates at the top of the wood layer. In this process, the seawater

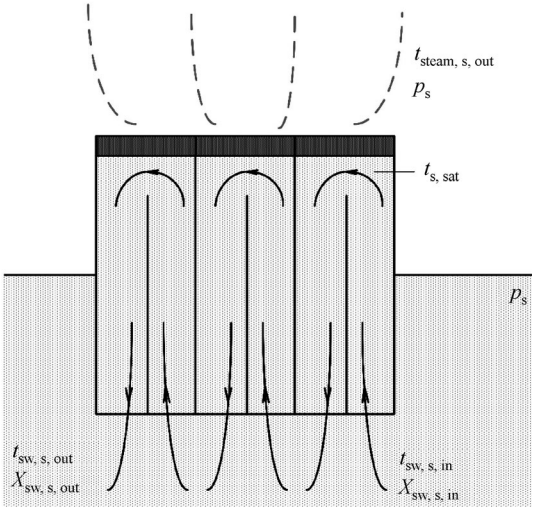

Fig. 3 Microcosmic operation of the bilayer wood solar steam generation

absorbs heat from the top layer and evaporates at the saturation temperature determined by the pressure inside the tank, so that steam is produced. After that and in the third process, the brine with increased salinity dissolves back to the seawater chamber, while the steam is further heated, which is similar to the overheating phenomenon, and discharged from the collector to the steam chamber. Consequently, the performance of the solar steam generator depends on its operational parameters such as, seawater and the steam outflow, seawater inlet temperature, inlet and outlet salinity, operating pressure of the seawater and steam, as well as the solar absorption capacity and efficiency.

The modeling of the bilayer solar steam generation can be modeled as follows. The process of the seawater heating can be treated as an isobaric heating process, in which the seawater is heated from the inlet seawater temperature to saturation temperature at a constant pressure. The solar energy consumption can be calculated by

$$Q_1 = m_{\mathrm{sw,solar,in}} c_{\mathrm{p,sw}} \left(t_{\mathrm{sw,sat}}|_{p_{\mathrm{chamber}}} - t_{\mathrm{sw,solar,in}}\right), \quad (1)$$

$$t_{\mathrm{sw,sat}}|_{p_{\mathrm{chamber}}} = t_{\mathrm{sat}}|_{p_{\mathrm{chamber}}} + BPE|_{t_{\mathrm{sat}}, X_{\mathrm{sw,solar,in}}}, \quad (2)$$

where Q_1 is the energy consumption in the first process, kJ; $m_{\mathrm{sw,solar,in}}$ is the mass flow rate of seawater at the inlet, $\mathrm{kg \cdot s^{-1}}$; $c_{\mathrm{p,sw}}$ is the isobaric specific heating capacity of seawater, $\mathrm{kJ \cdot kg^{-1} \cdot K^{-1}}$; $t_{\mathrm{sw,sat}}|_{p_{\mathrm{chamber}}}$ is the saturation seawater temperature at the chamber pressure, K; $t_{\mathrm{sw,solar,in}}$ is the seawater temperature at the inlet, K; and $BPE|_{t_{\mathrm{sat}}, X_{\mathrm{sw,solar,in}}}$ is the boiling temperature elevation at the saturation temperature and salinity, K.

The evaporation process can be modeled as an isobaric process. The amount of heat supplied to evaporation depends on the salinity of the seawater, steam flow rate, and operating pressure. This process could be described as

$$\mathrm{d}Q_2 = -\mathrm{d}m\left(h_{\mathrm{vapor,sat}}|_{p,X} - h_{\mathrm{liquid,sat}}|_{p,X}\right), \quad (3)$$

$$\frac{X}{X + \mathrm{d}X} = \frac{m + \mathrm{d}m}{m}, \quad (4)$$

where Q_2 is the energy consumption in the second process, kJ; $h_{\mathrm{vapor,sat}}|_{p,X}$ is the vapor saturation specific enthalpy at the given pressure and salinity, $\mathrm{kJ \cdot kg^{-1}}$; $h_{\mathrm{liquid,sat}}|_{p,X}$ is the liquid saturation specific enthalpy at the given pressure and salinity, $\mathrm{kJ \cdot kg^{-1}}$.

The steam-heating process can be modeled as an isochoric process. The amount of energy consumed can be calculated with the suction pressure and discharge pressure

$$Q_3 = m_{\mathrm{steam}}\left(h|_{v,p_{\mathrm{dis}}} - h|_{v,p_{\mathrm{suc}}}\right), \quad (5)$$

where Q_3 is the energy consumption in the third process, kJ; m_{steam} is the mass flow rate of steam; $h|_{v,p_{\mathrm{dis}}}$ is the specific enthalpy of steam at the discharge pressure and specific volume, $\mathrm{kJ \cdot kg^{-1}}$; and $h|_{v,p_{\mathrm{suc}}}$ is the specific enthalpy of steam at the suction pressure and specific volume, $\mathrm{kJ \cdot kg^{-1}}$.

The total solar energy consumption of the bilayer solar steam generation is the sum of the thermal energy consumed in the three processes divided by the solar absorption efficiency at the top black layer of the bilayer wood.

$$Q_{\mathrm{solar}} = (Q_1 + Q_2 + Q_3)/\eta_{\mathrm{solar}}, \quad (6)$$

where Q_{solar} is the heating capacity of solar collector, kJ; and η_{solar} is the solar collecting efficiency.

3 Configuration of MED system

The bilayer wood solar steam generator can supply the necessary thermal energy associated with the steam to drive the MED plant, as depicted in Fig. 4.

The MED system is composed of an ejector, falling film evaporators, preheaters, heat recovery exchangers, flash tanks, and a seawater reservoir. The falling film evaporator is a core component of the MED system, in which the seawater is sprayed onto a series of tubes and evaporates. The tubes serve as a heat exchanger between the condensation of the steam inside the tubes and the evaporation of salinity water outside the tubes. The flash tank with the expansion valves generates the steam supplied to the preheater. The preheater is used to heat up the seawater. The steam ejector compresses the low-pressure vapor from the last effect back to the first effect. The motive steam of the ejector is produced by the proposed bilayer wood steam generator. The variable speed pumps control the flow rate of the outlet steam and

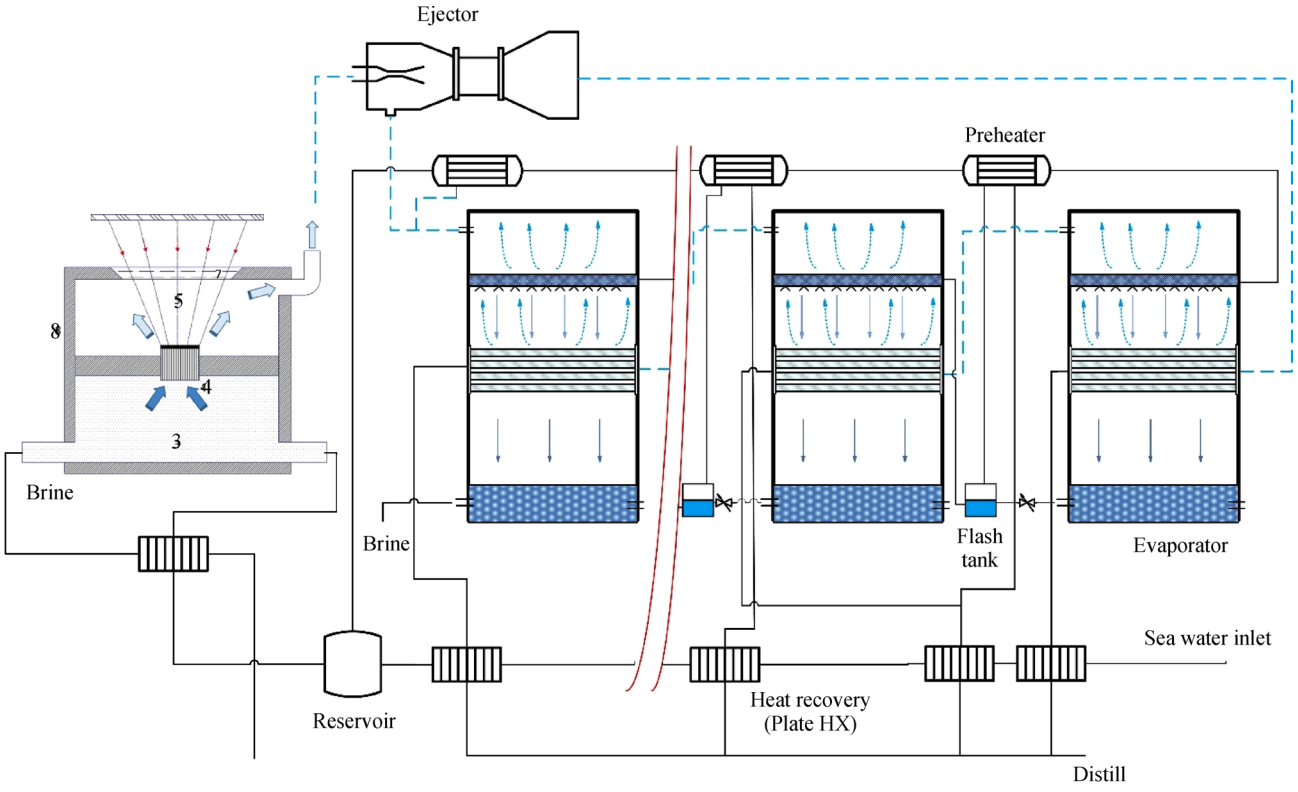

Fig. 4 Schematic diagram of a MED process combined with a steam ejector (The steam ejector compresses the low-pressure vapor from the last effect back to the first effect. The motive steam of the ejector is produced by the proposed bilayer wood steam generator.)

the inlet seawater to maintain the desired temperature and pressure level of the system.

4 Modeling of the MED plant combined with the bilayer solar steam generator

4.1 Energy and mass balance equations

In the MED system, each component can be modeled as a control volume with fluids flowing in or out, salinity changes, as well as heat and power consumed. The basic equations describing the mass balance and energy balance are given as

$$\sum_{\text{in}} \dot{m} = \sum_{\text{out}} \dot{m}, \tag{7}$$

$$\dot{Q} - \dot{W} + \sum_{\text{in}} \dot{m}h - \sum_{\text{out}} \dot{m}h = 0, \tag{8}$$

$$m_{\text{f}} = m_{\text{dis}} + m_{\text{brine}}, \tag{9}$$

$$x_{\text{f}} m_{\text{f}} = x_{\text{brine}} m_{\text{brine}}, \tag{10}$$

where m_{f} is the mass flow rate of fluid, $\text{kg}\cdot\text{s}^{-1}$; m_{dis} is the discharged vapor mass flow rate, $\text{kg}\cdot\text{s}^{-1}$; m_{brine} is the brine mass flow rate, $\text{kg}\cdot\text{s}^{-1}$; x_{f} is the salinity of fluid; and x_{brine} is the salinity of brine.

The following assumptions are made to simplify the thermodynamic analysis of the MED system.

(1) Steady-state assumption. All components are at steady-state and dynamic characteristics are neglected.

(2) All throttling processes are viewed as isenthalpic processes.

(3) The pressure loss within heat exchangers is neglected.

(4) The heat leakage from the solar collector system is neglected.

4.2 Ejector

The main part of the steam ejector is the nozzle zone. The correlation used for the steam jet ejector is [24],

$$Ra = 0.296 \frac{(P_{\text{s}})^{1.19}}{(P_{\text{ev}})^{1.04}} \left(\frac{P_{\text{motive}}}{P_{\text{ev}}}\right)^{0.015} \left(\frac{PCF}{TCF}\right), \tag{11}$$

$$Ra = \frac{m_{\text{motive}}}{m_{\text{ev}}}, \tag{12}$$

$$PCF = 3 \times 10^{-7} (P_{\text{motive}})^2 - 0.0009 P_{\text{motive}} + 1.6101, \tag{13}$$

$$TCF = 2 \times 10^{-8}(T_{ev})^2 - 0.0006T_{ev} + 1.0047, \quad (14)$$

where Ra is the entrainment ratio of flow rate; P_s is the discharge pressure; P_{ev} is the pressure of entrained vapor, kPa; P_{motive} is the pressure of motive vapor, kPa; PCF is the pressure correction factor; TCF is the temperature correction factor; T_{ev} is the temperature of entrained vapor, °C. This correlation is valid when $Ra < 4$, $10°C < T_{ev} < 500°C$, 100 kPa $< P_{motive} <$ 3500 kPa, and $P_s/P_{ev} > 1.81$. This correlation is capable of determining the mass flow of the motive steam according to the required mass flow of the entrained vapor, when the motive steam pressure, the discharge pressure and the suction pressure are given.

4.3 Evaporator

The heat transfer rate in the evaporator is determined by the falling film evaporation outside the tube, the convection, or the condensation of steam inside the tube, and the heat conduction of the tube wall, which is given by

$$\kappa_i = 1/\left[\left(R_{in} + \frac{1}{\alpha_{in}}\right)\frac{d_{out}}{d_{in}} + \frac{d_{out}}{2\lambda}\ln\left(\frac{d_{out}}{d_{in}}\right) + \left(R_{out} + \frac{1}{\alpha_{out}}\right)\right], \quad (15)$$

where κ_i is the heat transfer rate, $W \cdot m^{-2} \cdot K^{-1}$; R_{in} and R_{out} are the fouling resistance of inner and outer pipe wall respectively, $m^2 \cdot K^{-1} \cdot W^{-1}$; d_{in} and d_{out} are the inner and outer diameter of pipelines respectively, m; α_{in} and α_{out} are the inner and outer heat transfer coefficient respectively, $W \cdot m^{-2} \cdot K^{-1}$; and λ is the heat conductivity coefficient, $W \cdot m^{-2} \cdot K^{-1}$.

The heat transfer coefficients of each effect distiller are described by the following equations [10,25].

The falling film evaporation outside the tube is given by

$$\alpha_{out} = 0.032\left(\lambda_l^3 g/\nu_l^2\right)^{\frac{1}{3}}(4\Gamma/\mu_l)^{0.3367}\mathrm{Pr}^{0.4629}, \quad (16)$$

$$\Gamma = \frac{F}{L \cdot N}, \quad (17)$$

where α_{out} is the outer heat transfer coefficient, $W \cdot m^{-2} \cdot K^{-1}$; λ_l is the heat conductivity coefficient of liquid, $W \cdot m^{-2} \cdot K^{-1}$; ν_l is the specific volume of liquid, $m^3 \cdot kg^{-1}$; μ_l is the dynamic viscosity of liquid, Pa·s; F is the flow rate, $kg \cdot h^{-1}$; L is the length of tubes, m; and N is the number of tubes.

The condensation heat transfer inside the tube is given by

$$\alpha_{in} = 0.555\left\{\lambda_l^3 \rho_l(\rho_l - \rho_v)g\left[r + \frac{3}{8}c_{p,l}(T_{sat} - T_w)\right]\left[\mu_l d_{in}(T_{sat} - T_w)\right]\right\}^{\frac{1}{4}}, \quad (18)$$

where α_{in} is the inner heat transfer coefficient, $W \cdot m^{-2} \cdot K^{-1}$; λ_l is the heat conductivity coefficient of liquid, $W \cdot m^{-2} \cdot K^{-1}$; ρ_l and ρ_v are the density of liquid and vapor respectively, $kg \cdot m^{-3}$; r is latent heat, $kJ \cdot kg^{-1}$; T_{sat} is saturation temperature, K; T_w is the wall temperature, K; μ_1 is the dynamic viscosity of liquid, Pa·s; and d_{in} is the inner diameter of pipelines, m.

The convective heat transfer coefficient of the single phase flow in tubes is given by

$$Nu = 0.023\mathrm{Re}^{0.8}\mathrm{Pr}^n, \quad (19)$$

where $n = 0.4$ for heated situation and $n = 0.3$ otherwise. Therefore, the heat transfer capacity of the evaporator can be calculated by

$$Q = \kappa A \Delta T. \quad (20)$$

4.4 Preheater

Heat transfer coefficient of vapor condensation in tubes is determined by [10,26]

$$\alpha_{in} = 0.725\left[\frac{g r \rho_l^2 \lambda_l^3}{\mu_l d_{in} N(T_{sat} - T_w)}\right]^{\frac{1}{4}}, \quad (21)$$

where α_{in} is the inner heat transfer coefficient of preheater, $W \cdot m^{-2} \cdot K^{-1}$.

The average heat transfer coefficient of seawater convection could be determined with the average Nusselt number given by Chuichill as [26]

$$Nu = 0.3 + \frac{0.62\mathrm{Re}^{0.5}\mathrm{Pr}}{\left[1 + (0.4\mathrm{Pr}/)^{\frac{2}{3}}\right]^{0.25}}\left[1 + \left(\frac{\mathrm{Re}}{2.82 \times 10^5}\right)^{0.625}\right]^{0.8}, \quad (22)$$

valid for $0.7 < \mathrm{Pr} < 500$ and $30 < \mathrm{Re} < 10^8$.

4.5 Boiling temperature elevation

The boiling temperature elevation of seawater with different salinity is given by [27]

$$BPE = AX + BX^2 + CX^3,$$

$$A = 8.325 \times 10^{-2} + 1.883 \times 10^{-4}T + 4.02 \times 10^{-6}T^2,$$

$$B = -7.625 \times 10^{-4} + 9.02 \times 10^{-5}T - 5.2 \times 10^{-7}T^2,$$
$$C = 1.522 \times 10^{-4} - 3 \times 10^{-6}T - 3 \times 10^{-8}T^2, \quad (23)$$

where X is the salinity and T is the seawater temperature.

4.6 Simulation flowchart

The geometric and operating parameters for the MED system combined with the bilayer solar steam generator are listed in Table 1. Figure 5 demonstrates the flowchart for the simulation of the MED system combined with the bilayer solar steam generator. The simulation starts from assigning the steam flow rate at the outlet of last effect. With the assigned outlet salinity, the thermodynamic properties of the last effect, including the evaporation temperature, the heating capacity, and the BPE, could be calculated. With the evaporator model stated above, the calculation of the heat exchanging capacity of the last effect could be made. Step by step, a similar process could be conducted on each effect of desalination, and the inlet salinity of seawater is then determined. Afterwards, the ejector model is employed to calculate the seawater inlet temperature, thus the solar heating capacity. Finally, with the converged results on the steam flow rate, all calculation results could be calculated and output. In this investigation, Matlab R2017a is employed as the solver.

Table 1 Geometric and operating parameters

Parameters	Value
Inlet seawater salinity/%	4.2
Inlet seawater temperature/°C	25
Outlet brine temperature/°C	35
Number of tube	20 (4 × 5)
Energy efficiency of preheater	0.9
Inner diameter of tubes/mm	20
Outer diameter of tubes/mm	30
Length of tubes/m	1
Area of preheater/m^2	2

5 Results and discussion

5.1 Influence of brine flowrate

The brine flow rate is a critical operating parameter that determines the performance of the forward feed MED system. If the brine flow rate is too low, the salinity in those evaporators increases and then the BPE increases. As a result, the MED system will have fewer effects and therefore produce less distilled water when the inlet seawater temperature and the outlet steam temperature are held constant. On the other hand, if the brine flow rate is too large, the inlet seawater may not be heated up to the saturation temperature in the preheater and the steam generation is severely reduced. Therefore, the brine flow rate needs to be optimized to maximize the fresh water production in the MED system. The brine discharge flow rate takes both the seawater inlet flow rate and the discharge salinity control into account. In this investigation, the influence of brine outflow rate on performances is analyzed.

The influence of brine flow rate on system performance is displayed in Fig. 6. Figure 6(a) shows the distill flow rate and specific energy consumption as a function of the brine flow rate for different number of effects in the MED system with a solar absorbing capacity of 100 kW and a steam discharge temperature of 140°C. It can be seen that that the distilled water flow rate declines rapidly with the increase in the brine water flow rate in the MED system with 30 effects. On the contrary, the distilled water flow rate increases with the increase in the brine water flow rate in the MED system with 10 effects. The difference should come from the evaporation temperature, as is presented in Fig. 6(c). When the flow rate is larger, the preheating energy consumption significantly increases while the solar collector is less efficient in producing steam. However, at a lower evaporation temperature, the efficiency of desalination is influenced by the salinity of brine, which is the situation for the 10 effect system. The specific power consumption under the given operating condition can be as low as 23.61 kWh for each ton of fresh water product, but it will increase significantly with the changes in the brine flow rate and the number of effects in the MED system. Figure 6(c) exhibits the evaporation temperature in the first-effect evaporator as a function of brine flow rate for different number of effects in the MED system with a solar absorbing capacity of 100 kW and a steam discharge temperature of 140°C. It can be seen that the evaporation temperature decreases significantly with the increase in the brine flow rate. For example, the evaporation temperature decreases from 129.13°C to 69.96°C when the brine flow rate increases from 0.1 kg/s to 1 kg/s for the 20 effect.

Figures 6(b) and 6(d) show the influence of brine flow rate on system performance in the MED system with a solar absorbing capacity of 30 kW. The curves of distilled water rate and specific energy consumption in Fig. 6(b) are very different from those in Fig. 6(a). It can been seen in Fig. 6(b) that the distilled fresh water flow rate increases, reaches a maximum, and then decreases, as the brine flow rate increases. Interestingly, the specific energy consumption in the MED system with the 20–30 effects and 30 kW heating capacity is lower than that for the MED system with a heating capacity of 100 kW. The difference between the 30 kW and 100 kW system may result from its sensitivity to salinity changes in the evaporation. When the capacity is larger, the salinity increases more rapidly

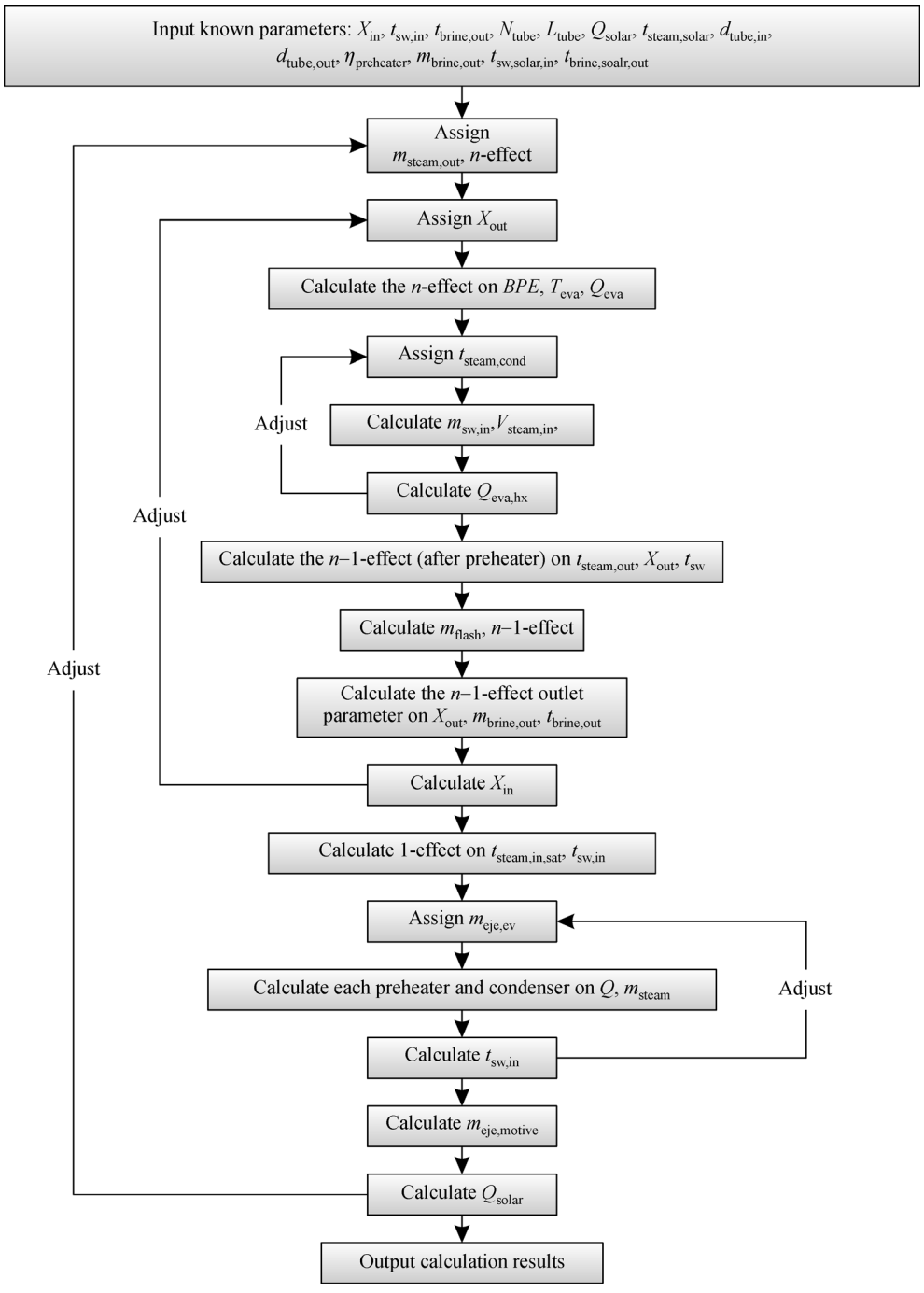

Fig. 5 Simulation flowchart for the MED desalination system

between effects, so that the BPE increases to lower the evaporation temperature in the next effect. Therefore, a profound system should take both the capacity and seawater flow into consideration for optimal operating condition.

5.2 Influence of steam temperature

The temperature of the steam, produced by the bilayer wood solar steam generator to drive the MED system, is another critical parameter that determines the system performance. In general, increasing the steam temperature in the solar collector system will lead to more loss in thermal energy in the seawater preheating. On the other hand, when the motive steam temperature increases, the evaporation temperature of the first effect can be increased, so that more effects of evaporation can be added to the MED system. Therefore, the steam temperature can be

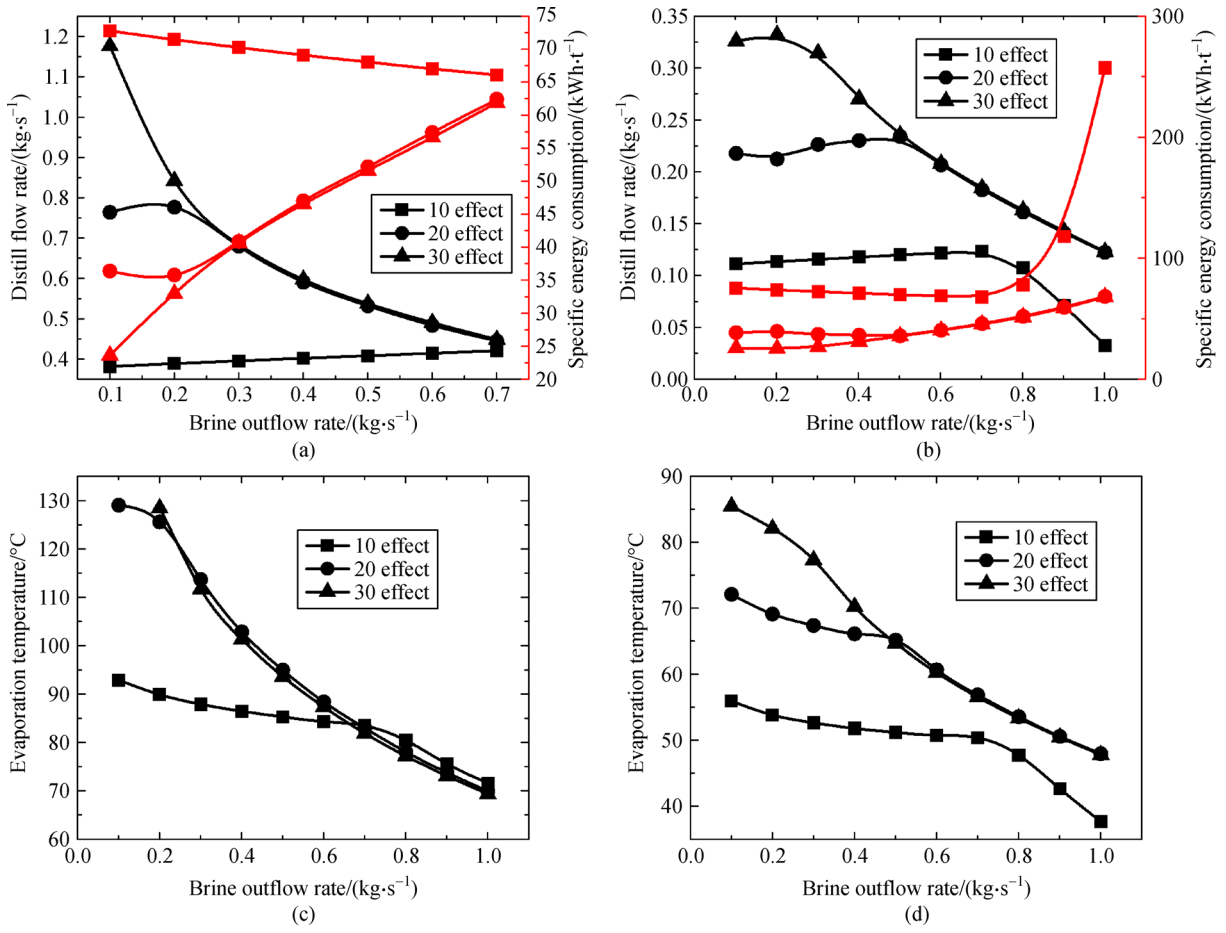

Fig. 6 Influence of brine flow rate on system performance

(a) Distill flow rate (black) and specific energy consumption (red) at Q_{solar} = 100 kW; (b) distill flow rate (black) and specific energy consumption (red) at Q_{solar} = 30 kW; (c) evaporation temperature of first effect at Q_{solar} = 100 kW; (d) evaporation temperature of first effect at Q_{solar} = 30 kW

optimized to enhance the performance of the MED system.

Figure 7 shows the changes of optimal number of effects for minimum specific power consumption with the temperature of the motive steam in the MED system. The solar absorbing capacity of the MED system is selected as 100 kW while the brine outflow rate is 0.3 kg/s. It is observed that the specific power consumption first decreases from 33.92 kWh/t to a minimum 24.88 kWh/t, and then increases to 27.06 kWh/t, when the motive steam temperature increases from 125°C to 160°C. The optimal temperature of the motive steam is found to be 145°C to minimize the specific energy consumption. The optimal number of effects increases monotonically with the increasing steam temperature.

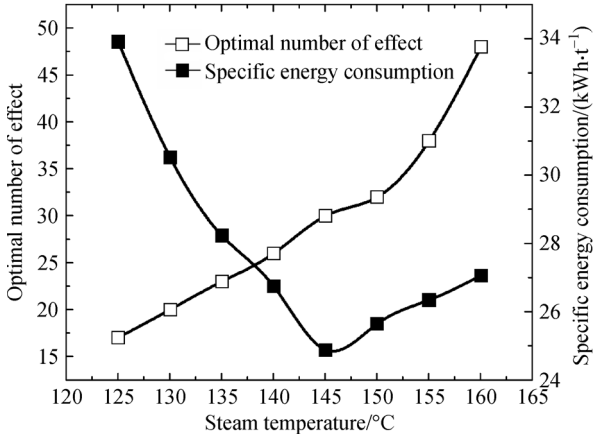

Fig. 7 Optimal number of effects and specific energy consumption as a function of solar steam temperature

5.3 Influence of input solar energy

Figure 8 shows the influence of input solar energy on the performance of the MED system at a constant brine outflow rate of 0.3 kg/s and a constant discharge steam temperature of 140°C. It can be seen that the fresh water production increases monotonically with the increase in the input solar energy. The specific power consumption decreases first and then reaches a constant when the input solar energy increases. The reason for such changes also

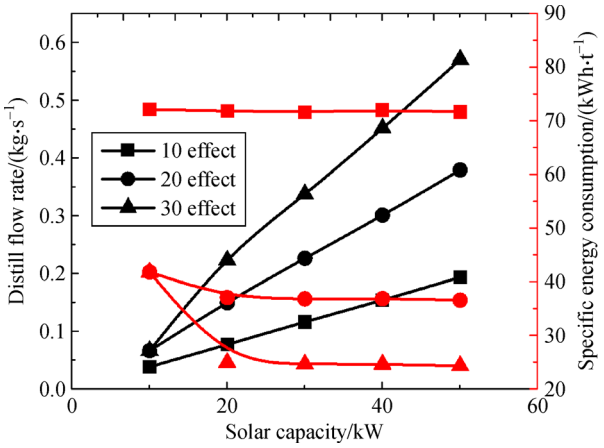

Fig. 8 Influence of input solar energy

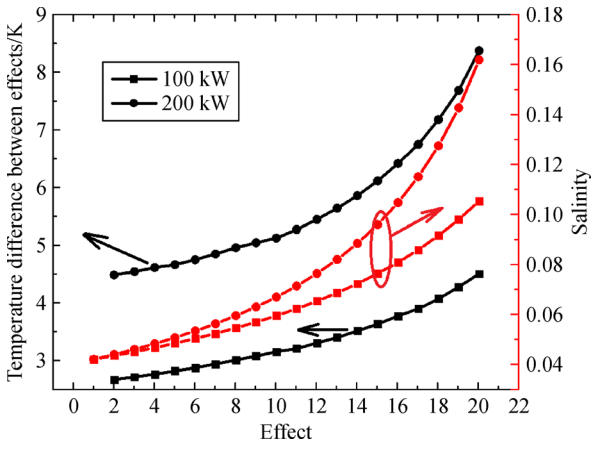

Fig. 9 Temperature difference between effects and salinity in each effect

comes from the influence of preheating for steam producing in solar collector and the salinity changes between effects. With the increase in solar capacity, specifically less energy is wasted on seawater heating in the tank, so that the specific energy consumption decreases. However, it does not continue to decrease because the increase in salinity may be much more significant, which leads to the increase in evaporation temperature in the first effect, and entrains less vapor in the ejector. Consequently, the optimal solar capacity should take the flow rate and heat exchange capacity into consideration.

5.4 Temperature differences between effects

Figure 9 illustrates the evaporation temperature and salinity in each effect of the MED system operating at a brine outflow rate of 0.3 and a discharge steam temperature of 140°C. The temperature difference between two adjacent effects increases from the first to the last effect of the evaporators. The temperature difference between two adjacent effects ranges from 4.48°C to 8.37°C in the MED system with a solar absorbing capacity of 200 kW, while the temperature difference ranges from 2.67°C to 4.5°C in the MED system with a solar absorbing capacity of 100 kW. The reason for this is that the salinity increases from the first effect to the last effect, which leads to an increase in BPE.

6 Conclusions

This paper presents a parametric study for the MED system driven by a newly discovered bilayer wood solar steam generator. A thermodynamic model has been developed to analyze the performance of the bilayer wood solar steam generator and the MED system driven by the bilayer wood steam generator. Models for falling film evaporator, preheater, ejector, and brine thermodynamic properties have been introduced to the system model. The effects of operating parameters, such as the motive steam temperature, seawater flow rate, input solar energy, and number of effects on the energy consumption for each ton of distilled water produced have been investigated in the MED system combined with the bilayer wood solar steam generator. It is found that, under a given operating condition, there exists an optimum steam generation temperature of around 145°C in the wood solar collector, so that the specific power consumption in the MED system reaches a minimum value of 24.88 kWh/t. The brine flow rate is also found to have a significant effect on the specific energy consumption. The energy consumption increases rapidly with the increase in the brine water flow rate in the MED system with 30 effects, while it decreases in the MED system with 10 effects. This parametric simulation study will help the design of efficient bilayer wood solar steam generator as well as the MED desalination system.

Acknowledgements This work was financially supported by the National Science Foundation in US (award #1706777) and China Scholarship Council.

Notations

A	Area /m^2
BPE	The rise in brine's boiling point rise/K
d	Diameter/m
F	Mass flow rate/(kg·s^{-1})
h	Specific enthalpy/(kJ·kg^{-1})
m	Refrigerant mass/kg
N	Number
P	Pressure/kPa

Q	Heat/kJ
R	Fouling resistance of pipe wall/($m^2 \cdot K^{-1} \cdot W^{-1}$)
r	Latent heat/($kJ \cdot kg^{-1}$)
T	Temperature/K
W	Power consumption/kJ
X	Salinity
α	Heat transfer coefficient/($W \cdot m^{-2} \cdot K^{-1}$)
λ	Heat transfer coefficient/($W \cdot m^{-2} \cdot K^{-1}$)
μ	Dynamic viscosity/($Pa \cdot s$)
ρ	Density/($kg \cdot m^{-3}$)
dis	Discharge
ev	Entrained vapor
f	Fluid
l	Liquid
sat	Saturation
sw	Seawater
suc	Suction
v	Vapor
w	Wall

References

1. Khawaji A D, Kutubkhanah I K, Wie J M. Advances in seawater desalination technologies. Desalination, 2008, 221(1–3): 47–69
2. Ghaffour N, Missimer T M, Amy G L. Technical review and evaluation of the economics of water desalination: current and future challenges for better water supply sustainability. Desalination, 2013, 309: 197–207
3. Elimelech M, Phillip W A. The future of seawater desalination: energy, technology, and the environment. Science, 2011, 333(6043): 712–717
4. Cipollina A, Micale G, Rizzuti L. Seawater Desalination: Conventional and Renewable Energy Processes. Berlin: Springer, 2009
5. Al-Karaghouli A, Kazmerski L L. Energy consumption and water production cost of conventional and renewable-energy-powered desalination processes. Renewable & Sustainable Energy Reviews, 2013, 24: 343–356
6. Al-Nory M, El-Beltagy M. An energy management approach for renewable energy integration with power generation and water desalination. Renewable Energy, 2014, 72: 377–385
7. Elminshawy N A S, Siddiqui F R, Sultan G I. Development of a desalination system driven by solar energy and low grade waste heat. Energy Conversion and Management, 2015, 103: 28–35
8. Reddy K V, Ghaffour N. Overview of the cost of desalinated water and costing methodologies. Desalination, 2007, 205(1–3): 340–353
9. Darwish M A, Al-Juwayhel F, Abdulraheim H K. Multi-effect boiling systems from an energy viewpoint. Desalination, 2006, 194 (1–3): 22–39
10. Zhang F M, Xu S M, Feng D D, Chen S Q, Du R X, Su C J, Shen B Y. A low-temperature multi-effect desalination system powered by the cooling water of a diesel engine. Desalination, 2017, 404: 112–120
11. Zhang Y, Sivakumar M, Yang S Q, Enever K, Ramezanianpour M. Application of solar energy in water treatment processes: a review. Desalination, 2018, 428: 116–145
12. Sun J, Liu Q B, Hong H. Numerical study of parabolic-trough direct steam generation loop in recirculation mode: characteristics, performance and general operation strategy. Energy Conversion and Management, 2015, 96: 287–302
13. Li L, Sun J, Li Y S. Thermal load and bending analysis of heat collection element of direct-steam-generation parabolic-trough solar power plant. Applied Thermal Engineering, 2017, 127: 1530–1542
14. Bataineh K M. Multi-effect desalination plant combined with thermal compressor driven by steam generated by solar energy. Desalination, 2016, 385: 39–52
15. Sharaf M A, Nafey A S, García-Rodríguez L. Thermo-economic analysis of solar thermal power cycles assisted MED-VC (multi effect distillation-vapor compression) desalination processes. Energy, 2011, 36(5): 2753–2764
16. El-Nashar A M. The economic feasibility of small MED seawater desalination plants for remote arid areas. Desalination, 2001, 134(1): 173–186
17. Al-Mutaz I S, Wazeer I. Current status and future directions of MED-TVC desalination technology. Desalination and Water Treatment, 2014, 55(1):1–9
18. Zhao D, Xue J, Li S, Sun H, Zhang Q D. Theoretical analyses of thermal and economical aspects of multi-effect distillation desalination dealing with high salinity waste water. Desalination, 2011, 273 (2–3): 292–298
19. ScienceDaily. Solar-powered devices made of wood could help mitigate water scarcity crisis. 2017–10–17, https://www.sciencedaily.com/releases/2017/10/171010224556.htm
20. The Chemical Engineer. Wood improves solar steam generation. 2017–11–16, https://www.thechemicalengineer.com/news/wood-improves-solar-steam-generation/
21. Zhu M, Li Y, Chen G, Jiang F, Yang Z, Luo X, Wang Y, Lacey S D, Dai J, Wang C, Jia C, Wan J, Yao Y, Gong A, Yang B, Yu Z, Das S, Hu L. Tree-inspired design for high-efficiency water extraction. Advanced Materials, 2017, 29(44): 1704107
22. Chen C, Li Y, Song J, Yang Z, Kuang Y, Hitz E, Jia C, Gong A, Jiang F, Zhu J Y, Yang B, Xie J, Hu L. Highly flexible and efficient solar steam generation device. Advanced Materials, 2017, 29(30): 1701756
23. Peng G, Ding H, Sharshir S W, Li X, Liu H, Ma D, Wu L, Zang J, Liu H, Yu W, Xie H, Yang N. Low-cost high-efficiency solar steam generator by combining thin film evaporation and heat localization: both experimental and theoretical study. Applied Thermal Engineering, 2018, 143: 1079–1084
24. Ding H, Peng G, Mo S, Ma D, Sharshir S W, Yang N. Ultra-fast vapor generation by a graphene nano-ratchet: a theoretical and simulation study. Nanoscale, 2017, 9(48): 19066–19072
25. Chiou J S, Yang S, Chen C K. Laminar film condensation inside a horizontal elliptical tube. Applied Mathematical Modelling, 1994,

18(6): 340–346
26. Churchill S W, Bernstein M. A correlating equation for forced convection from gases and liquids to a circular cylinder in crossflow. Journal of Heat Transfer, 1977, 99(2): 300–306
27. El-Dessouky H T, Ettouney H M. Fundamentals of Salt Water Desalination. Elsevier Science, 2002